frontiers | Frontiers in Astronomy and Space Sciences

TYPE Original Research
PUBLISHED 08 November 2023
DOI 10.3389/fspas.2023.1265919

OPEN ACCESS

EDITED BY
Yi Xu,
Horia Hulubei National Institute for Research and Development in Physics and Nuclear Engineering (IFIN-HH), Romania

REVIEWED BY
Canel Eke,
Akdeniz University, Türkiye
Marina Barbui,
Texas A&M University, United States

*CORRESPONDENCE
Wen Luo,
wenluo-ok@163.com
Weimin Zhou,
zhouwm@caep.cn

†These authors share first authorship

RECEIVED 24 July 2023
ACCEPTED 02 October 2023
PUBLISHED 08 November 2023

CITATION
Zhang J, Qi W, Fan W, Cao Z, Luo K, Tan C, Zhang X, Deng Z, Zhang Z, Li X, Yuan Y, Luo W and Zhou W (2023), Study of the isomeric yield ratio in the photoneutron reaction of natural holmium induced by laser-accelerated electron beams.
Front. Astron. Space Sci. 10:1265919.
doi: 10.3389/fspas.2023.1265919

Study of the isomeric yield ratio in the photoneutron reaction of natural holmium induced by laser-accelerated electron beams

Jingli Zhang[1†], Wei Qi[2†], Wenru Fan[1], Zongwei Cao[1], Kaijun Luo[1], Changxiang Tan[1], Xiaohui Zhang[2], Zhigang Deng[2], Zhimeng Zhang[2], Xinxiang Li[1], Yun Yuan[1], Wen Luo[1]* and Weimin Zhou[2]*

[1]School of Nuclear Science and Technology, University of South China, Hengyang, China, [2]Science and Technology on Plasma Physics Laboratory, Laser Fusion Research Center, China Academy of Engineering Physics, Mianyang, China

Introduction: An accurate knowledge of the isomeric yield ratio (IR) induced by the photonuclear reaction is crucial to study the nuclear structure and reaction mechanisms. ^{165}Ho is a good candidate for the investigation of the IR since the Ho target has a natural abundance of 100% and the residual nuclide has a good decay property.

Methods: In this study, the photoneutron production of $^{164m, g}$Ho induced by laser-accelerated electron beams is investigated experimentally. The γ-ray spectra of activated Ho foils are off-line detected. Since the direct transitions from the ^{164m}Ho are not successfully observed, we propose to extract the IRs of the $^{164m, g}$Ho using only the photopeak counts from the ground-state decay.

Results: The production yields of $^{164m, g}$Ho are extracted to be $(0.45 \pm 0.10) \times 10^6$ and $(1.48 \pm 0.14) \times 10^6$ per laser shot, respectively. The resulting IR is obtained to be 0.30 ± 0.08 at the effective γ-ray energy of 12.65 MeV.

Discussion: The present data, available experimental data, and TALYS calculations are then compared to examine the role of the excitation energy. It is found that besides the giant dipole resonance, the excitation energy effect also plays a key role in the determination of the IRs.

KEYWORDS

isomeric yield ratio, photoneutron reaction, laser-accelerated electron beam, effective γ-ray energy, $^{164m, g}$Ho

1 Introduction

Nuclear isomers have been widely studied due to their fascinating applications, including medical imaging (Habs et al., 2011; Pan et al., 2021), nuclear clocks (Peik et al., 2021), and nuclear batteries (Prelas et al., 2014). They still play a crucial role in various aspects of astrophysical nuclear reactions (Hayakawa et al., 2008; Zilges et al., 2022). In many nuclear reactions, the residual nuclei have isomeric states with narrow energy levels and relatively long half-lives. The isomeric cross-section or yield ratio (IR) of high-spin to low-spin states of the residual nucleus provides valuable information

about nuclear structure and reaction mechanisms, such as the transfer of angular momentum, the spin dependence of nuclear level density, the amelioration in γ-ray transition theory, and tests of different models (Naik et al., 2016; Rahman et al., 2020). In addition, the IR plays a key role in calculating the total production cross-section of the residual products when the production cross-section of one isomer is known in advance.

The excitation energy and angular momentum of incident particles can significantly affect the IR values of the residual products. The IRs have been studied in nuclear reactions induced by different incident particles, such as photon (Rahman et al., 2016), proton (Hilgers et al., 2007), neutron (Luo et al., 2014), and alpha (Kim et al., 2015). Compared to other particles, photons carry a smaller angular momentum of $1\hbar$ or $2\hbar$. Furthermore, intense bremsstrahlung photons can be readily produced using radio-frequency (RF) electron accelerators. As a result, the photonuclear reactions seem to be a good tool to investigate the effect of the excitation energy on the IR. Kolev et al. (1995) deduced the experimental IRs of $(\gamma, 3n)^{110m,g}$In, $(\gamma, n)^{164m,g}$Ho, and $(\gamma, 3n)^{162m,g}$Ho by a bremsstrahlung source with an end-point energy of 43 MeV. Thiep et al. (2011) determined the IRs of ^{165}Ho$(\gamma, n)^{164m,g}$Ho and ^{175}Lu $(\gamma, n)^{174m,g}$Lu reactions in the bremsstrahlung energy region from 14 to 25 MeV. Do et al. (2013) measured the IRs of ^{164m,g}Ho and ^{162m,g}Ho via ^{165}Ho(γ, n) and ^{165}Ho(γ, 3n) reactions in the bremsstrahlung energy region from 45 to 65 MeV. It is noticeable that the available IRs for the ^{165}Ho$(\gamma, n)^{164m,g}$Ho reactions are still scarce. It particularly lacks experimental data in the energy region below 11 MeV. With the rapid development of high-intensity laser technology (Danson et al., 2019), laser–plasma interactions are used to study various nuclear phenomena (Schlenvoigt et al., 2008; Günther et al., 2022; Cao et al., 2023). Recently, the efficient production of nuclear isomers, including ^{113m,115m}In and ^{93m}Mo, has been studied experimentally using the laser-accelerated electron beam (e^- beam) (Feng et al., 2022; Fan et al., 2023 under review).

In this study, we experimentally investigate the production of ^{164m,g}Ho by laser-induced photoneutron reactions. The γ-ray spectra of the activated Ho foils are detected by an offline γ-ray spectrometry technique. Since the direct transitions from ^{164m}Ho were not successfully observed, we propose to extract the ground and isomeric yields of ^{164}Ho using only the photopeak counts from the ground-state decay. We should note that this approach differs from determining the counts of two photopeaks that directly characterize the isomeric and ground states. The IR value of ^{165}Ho$(\gamma, n)^{164m,g}$Ho is obtained for a given excitation energy. The present and similar literature data on IRs are compared to examine the role of excitation energy. Furthermore, the cross-section and IR curves of the ^{165}Ho$(\gamma, n)^{164m,g}$Ho reaction are calculated by the TALYS software to examine the compatibility of the theoretical model with the experimental data.

2 Experimental setup

The ^{164m,g}Ho production experiment was performed on the XingGuang-III laser facility at the Laser Fusion Research Center in Mianyang. The experimental setup is schematically shown in Figure 1A. An intense laser pulse with a duration of ~0.8 ps and energy of ~100 J was focused by an f/2.6 off-axis parabola (OAP) mirror (Robbie et al., 2018) onto a supersonic gas jet with a well-defined uniform density distribution (Feng et al., 2022). In the first stage of the experiment, high-charge multi-MeV e^- beams were produced during the laser–gas interactions. An image plate (IP) stack with a central hole was used to measure the spatial distribution of the laser-accelerated e^- beam. It should be noted that the IP stack is composed of seven IPs, with each IP being stuck on a tantalum foil with a thickness of 0.5 mm. Meanwhile, an electron magnetic spectrometer (EMS) was placed downstream of the IP stack to accurately diagnose the energy of the e^- beam passing through the central hole of the IP stack. In the second stage of the experiment, a metal stack composed of Ta foil and stacked Ho foils was installed, and both the IP stack and EMS were uninstalled. The Ta foil is 2 mm thick, in which energetic bremsstrahlung photons are generated. The stacked Ho foils used for activation have 10 layers in total, with each layer having a thickness of 1 mm and a natural abundance of 99.99% (Inagaki et al., 2020). During the activation, the bremsstrahlung radiations irradiate the Ho foils, successfully triggering photoneutron reactions and then producing a large number of ^{164m,g}Ho, as shown in Figure 1B. After the activation, the Ho foils are taken out from the target chamber of the XingGuang-III laser facility. The activation spectra are recorded using a high-purity germanium (HPGe) detector. The response of the HPGe detector has been well calibrated by standard γ-ray sources, including ^{60}Co, ^{152}Eu, ^{133}Ba, ^{226}Ra, ^{137}Cs, and ^{241}Am. In order to reduce the self-absorption effect induced by the stacked Ho foils, the 10 layers are spread out at the surface of the Al window of the HPGe detector.

3 Isomeric yield ratio determination

The temporal evolution of the numbers of nuclei that are formed in the isomeric and ground states is described by the following kinetic equations (Thiep et al., 2011):

$$\begin{cases} \dfrac{dN_m}{dt} = p_m - \lambda_m N_m, \\ \dfrac{dN_g}{dt} = p_g + \eta\lambda_m N_m - \lambda_g N_g, \end{cases} \tag{1}$$

where the subscripts m and g designate the isomeric and ground states of ^{164}Ho, respectively; p_m and p_g are the production rates leading to ^{164}Ho in the isomeric and ground states; N_m and N_g are the numbers of nuclei in the corresponding states; λ_m and λ_g are the constants of nuclear decay; and η is the transition coefficient from the isomeric state to the ground state. These equations describe the processes involved in the direct production of the desired isotopes during the target irradiation and the reduction of the number of nuclei as a result of their radioactive decay. The production rate p_x with x being the subscript m or g (similarly hereinafter) can be written as (Kolev et al., 1995)

$$p_x = N_0 \int_{E_{th}}^{E_{max}} \varphi(E_\gamma)\sigma_x(E_\gamma)dE_\gamma = N_0 \Phi \langle \sigma_x \rangle, \tag{2}$$

where N_0 is the number of target nuclei, $\varphi(E_\gamma)$ represents the bremsstrahlung photon flux; $\sigma_x(E_\gamma)$ is the reaction cross-section leading to the formation of ^{164}Ho in both the isomeric and ground states; E_{th} and E_{max} are the reaction threshold and bremsstrahlung end-point energy, respectively; $\Phi = \int_{E_{th}}^{E_{max}} \varphi(E_\gamma)dE_\gamma$ is the integrated

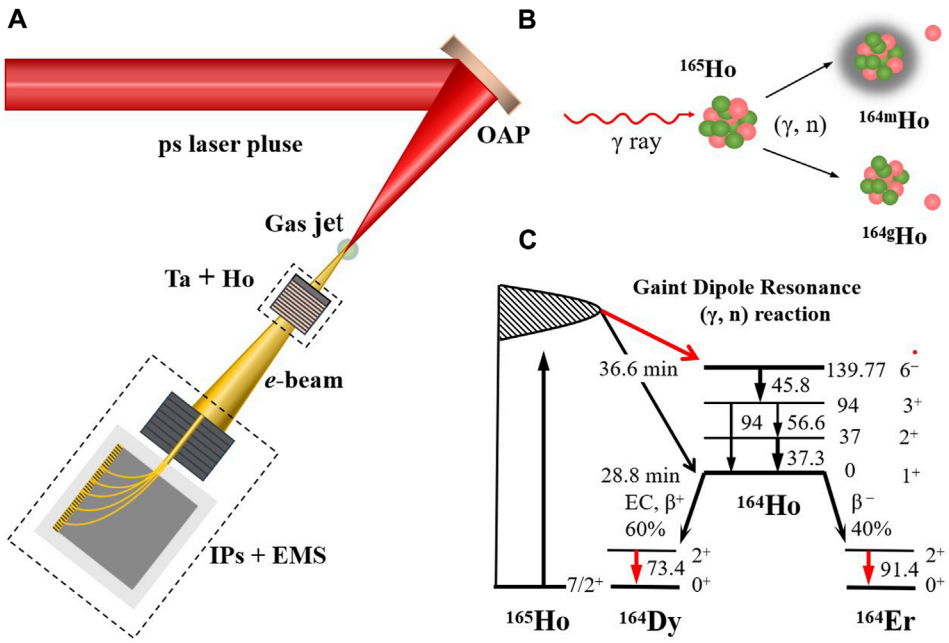

FIGURE 1
Experimental setup for the production of $^{164m,\,g}$Ho at the XingGuang-III laser facility (not to scale) **(A)**. Schematic view of the photoneutron production of $^{164m,\,g}$Ho **(B)** and the partial-level scheme of $^{164m,\,g}$Ho and the decay property of ^{164g}Ho (not to scale) **(C)**. As the laser-accelerated e^- beam fires to the metal stack (Ta + Ho), a large number of bremsstrahlung photons are generated, and subsequently, the Ho stacks are activated via photoneutron reactions, producing ^{164}Ho in both the ground state ($J^\pi = 1^+$) and isomeric state ($J^\pi = 6^-$) (Singh et al., 2018). The 6^- isomer in ^{164}Ho decays, via only internal decay, to the ground state. The decay from the 6^- isomer to the 3^+ excited state is an $E3$ transition. This 3^+ excited state subsequently de-excites to the ground state. The resulting transition energies are 94.0, 56.6, and 37.3 keV. Finally, the ground-state decays to the daughter nucleus ^{164}Dy or ^{164}Er, emitting two characteristic γ-rays at 73.4 and 91.4 keV.

photon flux; and $\langle\sigma_x\rangle = \int_{E_{th}}^{E_{max}}\varphi(E_\gamma)\sigma_x(E_\gamma)dE_\gamma / \int_{E_{th}}^{E_{max}}\varphi(E_\gamma)dE_\gamma$ is the flux-weighted average cross-section leading to the isomeric or ground state.

Since the gamma spectroscopy method is used in the experiment, the photopeak counts (C_x) of the characteristic γ-ray of interest can be readily obtained over the detection time t_d. When taking into account the irradiation time t_{irr} and the cooling time t_c, the solution of Eq. 1 in three time intervals (t_{irr}, t_c, and t_d) and the consequent integration of the relevant activity over the t_d lead to

$$C_m = I_m\varepsilon_m A p_m, \tag{3a}$$

$$C_g = I_g\varepsilon_g\left(Bp_g + Dp_m\right), \tag{3b}$$

where I_x and ε_x are the branching intensity and source-peak detection efficiency of the characteristic γ-rays to be detected, respectively. The other variables are listed as follows: $A = \frac{1}{\lambda_m}\left(1-e^{-\lambda_m t_{irr}}\right)e^{-\lambda_m t_c}\left(1-e^{-\lambda_m t_d}\right)$, $B = \frac{1}{\lambda_g}\left(1-e^{-\lambda_g t_{irr}}\right)e^{-\lambda_g t_c}\left(1-e^{-\lambda_g t_d}\right)$, and $D = \frac{\eta}{\lambda_g-\lambda_m}\left[\frac{\lambda_g}{\lambda_m}\left(1-e^{-\lambda_m t_{irr}}\right)e^{-\lambda_m t_c}\left(1-e^{-\lambda_m t_d}\right) - \frac{\lambda_m}{\lambda_g}\left(1-e^{-\lambda_g t_{irr}}\right)e^{-\lambda_g t_c}\left(1-e^{-\lambda_g t_d}\right)\right]$.

In the case of the bremsstrahlung photon, the expression of the IR reads (Jonsson et al., 1977) as follows:

$$IR = \frac{\langle\sigma_m\rangle}{\langle\sigma_g\rangle} = \frac{p_m}{p_g}. \tag{4}$$

Usually, the IR in a nuclear reaction is determined by measuring the counts of photopeaks that characterize the isomeric and ground states, respectively. When one or more photopeaks induced by the isomeric state are directly detected, the p_x and the resulting IR values can be readily obtained by solving Eq. 3 and Eq. 4, respectively (Rahman et al., 2020). In the case of the Ho sample, the photopeak at 37.3 keV is popularly used to characterize the isomeric state, while that at 73.4 and 91.4 keV is used to characterize the ground state, as shown in Figure 1C. In our experiment, the 37.3 keV photopeak was not successfully observed. This is because only single-shot irradiation is performed, and both the σ_m and ε_m values are relatively small. As a result, the abovementioned approach used to extract the IR value becomes invalid. It is shown in Eq. 3b that both the isomeric and ground states contribute to the C_g value, which varies with the t_d. It suggests that the p_x values can also be obtained by solving only Eq. 3b at two different time instants. More specifically, the p_x values can be deduced by solving the simultaneous equations of Eq. 3b at t_d^i and t_d^j, with i and j denoting two arbitrary time instants.

$$\begin{cases} p_g = \dfrac{D_j Y_i - D_i Y_j}{B_i D_j - B_j D_i}, \\ p_m = \dfrac{B_i Y_j - B_j Y_i}{B_i D_j - B_j D_i}, \end{cases} \tag{5}$$

where $Y_i = C_g^i / I_g\varepsilon_g$. This indicates that using only the photopeak counts from the ground-state decay, the IR value can be obtained. Furthermore, a group of data on IR can be obtained by reasonably changing the time increments. According to the error propagation, the uncertainties of the p_x values can be determined by the following

formula:

$$\begin{cases} \sigma(p_g) = \sqrt{\dfrac{D_j^2\sigma(Y_i)^2 + D_i^2\sigma(Y_j)^2}{(B_iD_j - B_jD_i)^2}}, \\ \sigma(p_m) = \sqrt{\dfrac{B_i^2\sigma(Y_j)^2 + B_j^2\sigma(Y_i)^2}{(B_iD_j - B_jD_i)^2}}. \end{cases} \tag{6}$$

As a result, the uncertainty of the *IR* value can be written as

$$\sigma(IR) = IR\sqrt{\frac{\sigma(p_g)^2}{p_g^2} + \frac{\sigma(p_m)^2}{p_m^2}}. \tag{7}$$

4 Results and discussion

4.1 Electron spectra

In our experiment, high-energy electrons are mainly produced by the parametrically enhanced direct laser acceleration (Cao et al., 2023). As the electron yield and charge are sensitive to the plasma density, the e^-beam generation can be optimized by adjusting the backing pressure of the gas jet. Figure 2A shows the energy distributions of truncated e^-beams recorded by the EMS at two backing pressures of 2.0 and 2.6 MPa. The spectral pattern of the e^-beam can be described by a Boltzmann distribution $\frac{dN}{dE} \propto e^{-\frac{E}{T_e}}$, where the T_e is the slope temperature (Qi et al., 2019). The fitting results show that the T_e values are 7.8 MeV and 4.8 MeV for backing pressures of 2.0 MPa and 2.6 MPa, respectively. In addition, the charge of the laser-accelerated electrons higher than 1 MeV is $Q_e \sim$ 42 nC at 2.0 MPa, which is 2.5 times higher than that at 2.6 MPa. The spatial distribution of the e^-beam is shown in Figure 2B. It is visibly seen that a bright spot is located beneath the central hole. According to the experimental arrangement and the spot size of the e^- beam, the laser-accelerated e^-beam has an angular divergence of approximately 200 mrad (FWHM).

Generally, only high-energy electrons can be used to induce isomer production. However, the bright electron spot is located beneath the central hole, as shown in Figure 2B. This suggests that most of the electrons with high energy did not pass through the central hole of the IP stack and were not recorded by the EMS in our experiment. To understand more about the spectral pattern of the laser-accelerated e^- beam, we utilized the Geant4 toolkit (Agostinelli et al., 2003) to simulate the attenuation of monoenergetic electrons inside the IP stack. For a given energy, when the number of incident electrons reduces by a factor of 0.9, such energy is regarded as the minimum energy recorded by each IP. Then, the spectral distribution of the e^- beam can be figured out but with a relatively large uncertainty. Similar studies have been conducted by Bonnet et al. (2013) and Nishiuchi et al. (2020). Figure 2C shows the simulated electron spectral distribution, which matches well with the Boltzmann distribution. Note that the uncertainty represents the detectable energy range for each IP. The slope temperature is fitted to be 16.2 MeV, which is two times higher than the one recorded by the EMS. This is because the bright e^- beam was not centered with the hole on the IP stack so that the EMS only detected the low-energy part of the e^- beam, as presented earlier. Since the slope temperature is sufficiently high, such an e^- beam interacting with a Ta foil can generate a high flux of bremsstrahlung radiation.

4.2 Characteristic γ-ray spectrum

The characteristic γ-rays emitted from the Ho sample were measured with the HPGe detector, as mentioned earlier. In our case, the cooling time t_c is 30 min. Figure 3A shows the measured characteristic γ-ray spectra for t_d = 240 min, from which two photopeaks at 73.4 keV (I_g = 1.88%) and 91.4 keV (I_g = 2.30%) are clearly observed, whereas the 37.3 keV γ-ray for ^{164m}Ho does not appear. This is because the amount of ^{164m}Ho produced during a single-shot irradiation was not enough to be detectable after the cooling time of 30 min. However, the signal and background counts around the γ-ray energy at 37.3 keV can be used to safely determine an upper limit for the yield of ^{164m}Ho. By integrating over the energy region of the characteristic γ-ray at 37.3 keV, the signal and background counts are 242, which gives an upper limit of 0.85×10^6 for the ^{164m}Ho yield according to Eq. 3a.

As mentioned previously, reasonably partitioning the C_g is vital to obtain the p_x and the resulting IR. The C_g values for 73.4 and 91.4 keV lines as functions of t_d are shown in Figure 3B. The temporal variation of C_g can be fitted well with Eq. 3b. The fitting curve can be re-written as

$$C_g = P_0e^{-\lambda_g t_d} + P_1e^{-\lambda_m t_d} + P_2, \tag{8}$$

where P_0, P_1, and P_2 are the coefficients dependent on the p_x. More specifically, the coefficients P_0 and P_2 are associated with both the p_m and p_g. P_1 is the function of p_m. From Eq. 8, one can see that the C_g value is not only contributed by the ground state of ^{164}Ho but also induced by its isomeric state. In our case, the P_1 is fitted to be −1865 ± 229, and the p_m value is then obtained to be $(0.44 \pm 0.05) \times 10^6$. The resulting confidence level is approximately 9.0 σ.

4.3 Isomeric ratio calculation

The calculation of the IR relies on the determination of p_m and p_g. Since the characteristic γ-ray line at 37.3 keV is not observed in our case, we employ the approach shown in Eq. 5 to extract the p_x values of ^{164m,g}Ho. Figure 4A presents 10 groups of p_x values obtained with the photopeak counts at 91.4 keV. The average $\overline{p_m}$ and $\overline{p_g}$ are calculated to be 0.45×10^6 and 1.48×10^6 per laser shot, respectively. The uncertainty of p_x is determined by $\sigma(p_x) = \sqrt{\sum_{i=1}^{i=n}\sigma_i^2(p_x)}/n$, where the $\sigma_i(p_x)$ is the uncertainty of p_x^i calculated by Eq. 6. Finally, the p_m and p_g of Ho produced in the experiment are obtained to be $(0.45 \pm 0.10) \times 10^6$ and $(1.48 \pm 0.14) \times 10^6$ per laser shot, respectively. Accordingly, the confidence level of p_m is 4.5 σ. It should be noted that the p_m value is in good agreement with the one obtained by fitting the C_g curve, as discussed earlier. However, its confidence level is smaller than the confidence level of P_1. This is reasonable since the former reasonably considers the error propagation. In addition, the p_m value is almost two times lower than the upper limit of 0.85×10^6 mentioned earlier, which in turn validates the feasibility of extracting the ^{164m}Ho yield using only the

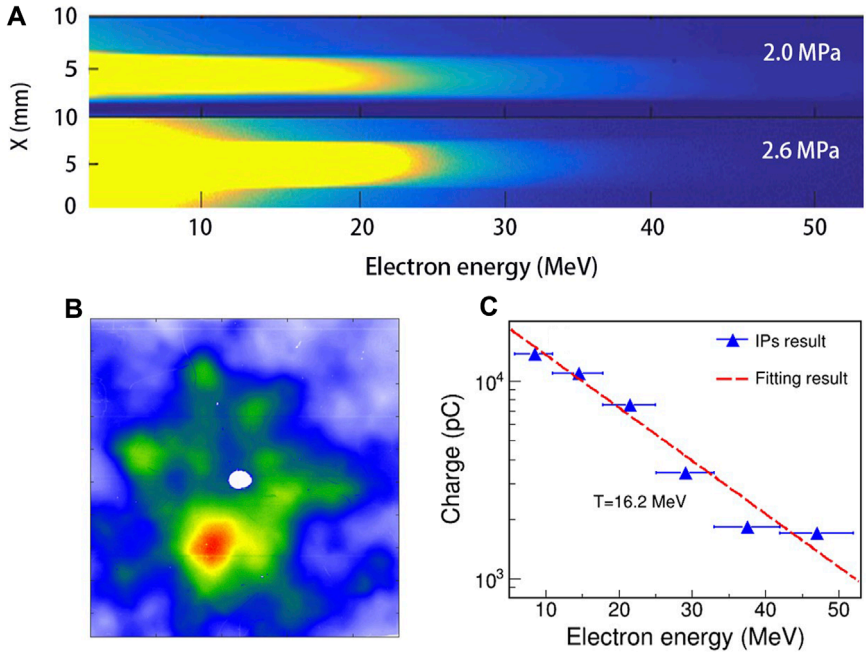

FIGURE 2
Spectral distributions of the laser-accelerated e^- beam diagnosed by the EMS **(A)**, spatial distribution of the laser-accelerated e^- beam recorded at the backing pressure of 2.0 MPa **(B)**, and the electron charge in dependence on the electron energy **(C)**.

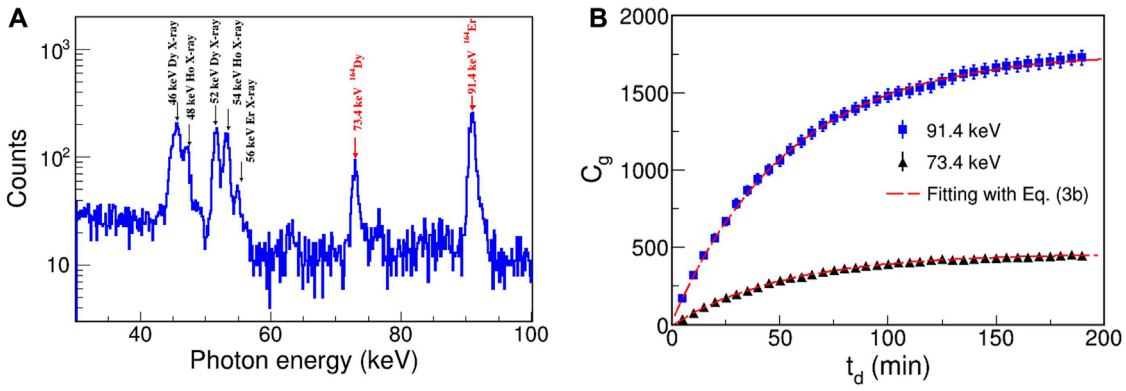

FIGURE 3
Typical γ-ray spectrum from the activated Ho foils (t_c = 30 min and t_d = 240 min) **(A)** and accumulated photopeak counts as a function of detection time **(B)**.

peak counts from the ground-state decay. Similarly, the *IR* value and its uncertainty $\sigma(IR)$ are calculated with Eq. 4 and 7, respectively. Figure 4B shows 10 groups of *IRs* and their average value. The *IR* value of ^{164m,g}Ho is 0.30 ± 0.08, which is less than unity. This is because the spin (J = 6) of the isomeric state is visibly higher than the ground state with J = 1.

Photoneutron reaction cross-section of ^{165}Ho calculated with TALYS 1.9 (Koning et al., 2019) and the data from the Experimental Nuclear Reaction Database (EXFOR) are compared and shown in Figure 5A. One can see that the ^{165}Ho(γ, n)^{164g}Ho reaction plays a dominant role in the giant dipole resonance (GDR) region. The ^{165}Ho(γ, n)^{164m}Ho reaction has a similar distribution with the ^{165}Ho(γ, n)^{164g}Ho. However, its maximum cross-section, ~60 mb, is visibly lower than that of the latter. As the photon energy continues to increase, the multiple emission reactions take over. The maximum cross-section decreases as the number of emitted particles increases. The TALYS calculations are in overall good agreement with the EXFOR data obtained from previous measurements using photon sources caused by positron annihilation in flight (Bergère et al., 1968; Berman et al., 1969). This indicates the reliability of the TALYS inputs and calculations. In addition, it is noticeable that the available experimental data in terms of isomer production are very rare, which can potentially be measured using state-of-the-art laser-Compton scattering facilities generating high-intensity and

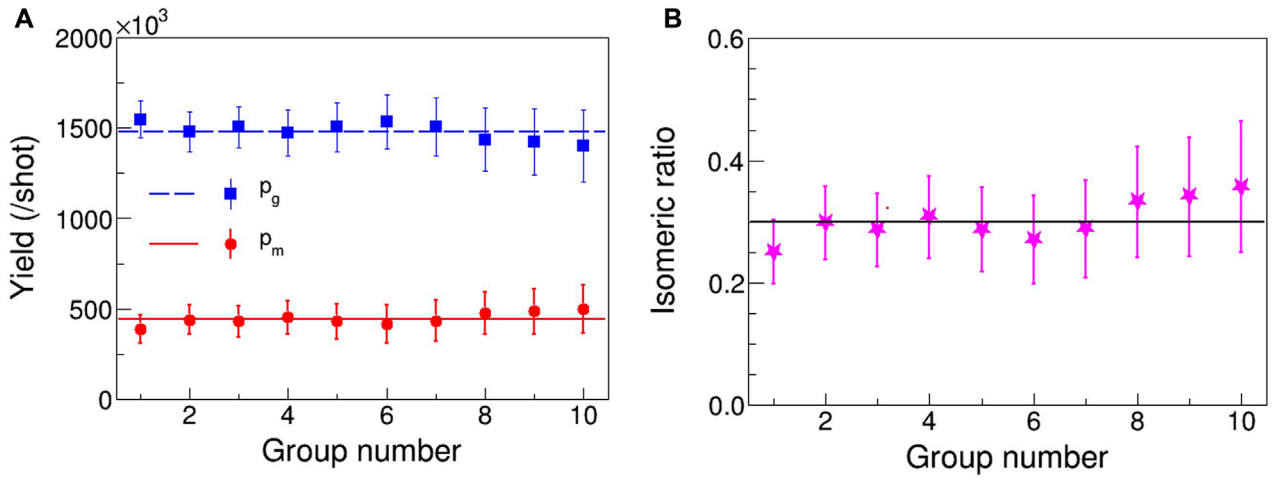

FIGURE 4
Ten groups of p_m, p_g **(A)**, and *IRs* **(B)** for the 91.4 keV photopeak. Group No. *i* (*i* = 1,2,……,10) indicates the data calculated with the photopeak counts at $t_d^i = 5i + 40$ min and $t_d^i = 5i + 120$ min. In **(A)**, the blue and red lines stand for the average $\overline{p_m}$ and $\overline{p_g}$, respectively. In **(B)**, the black line represents the average value of *IR* s.

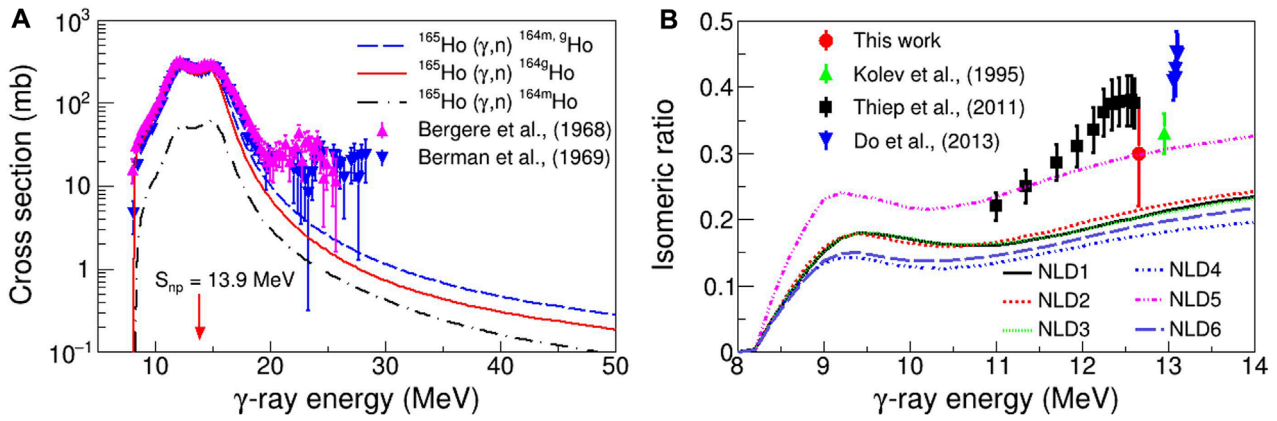

FIGURE 5
Calculated (γ, n) cross-sections for ^{165}Ho and the available EXFOR data for comparison **(A)** and the flux-averaged IR of $^{164m,\,g}$Ho in the ^{165}Ho(γ, n) reaction as a function of excitation energy **(B)**. In **(A)**, the experimental data are total cross-sections of the ^{165}Ho(γ, n) and ^{165}Ho(γ, np) reactions, and S_{np} denotes the threshold energy for the ^{165}Ho(γ, np) reaction. In **(B)**, the previous experimental data (Kolev et al., 1995; Thiep et al., 2011; Do et al., 2013) are obtained by bremsstrahlung photons from RF electron accelerators, and TALYS calculations considering different nuclear level density (NLD) models are also presented for comparison.

quasi-monoenergetic γ-ray beams (An et al., 2018; Wang et al., 2022).

The *IR*s of $^{164m,\,g}$Ho can be examined by using different bremsstrahlung radiations from both the laser-plasma accelerator and the RF accelerator. For this purpose, the effective γ-ray energy $\langle E_\gamma \rangle$ from the threshold to the end-point energy can be obtained by using the following relation (Jacobs et al., 1979):

$$\langle E_\gamma \rangle = \frac{\int_{E_{th}}^{E_{max}} \varphi(E_\gamma)\sigma_R(E_\gamma)E_\gamma dE_\gamma}{\int_{E_{th}}^{E_{max}} \varphi(E_\gamma)\sigma_R(E_\gamma)dE_\gamma}, \quad (9)$$

where the $\varphi(E_\gamma)$ is calculated with the Geant4 toolkit considering their realistic target arrangements, and $\sigma_R(E_\gamma)$ is the cross-section for the ^{165}Ho(γ, n)$^{164m,\,g}$Ho reaction, which is calculated by using the default option in the TALYS software. In order to understand the effect of excitation energy, the measured *IR* value of $^{164m,\,g}$Ho from the present work, literature values, and TALYS calculations are plotted in Figure 5B as a function of $\langle E_\gamma \rangle$. From the EXFOR data, one can see that when $\langle E_\gamma \rangle$ > 11 MeV, the *IR* of $^{164m,\,g}$Ho increases with the $\langle E_\gamma \rangle$ and then gets saturated. This is because the input angular momentum brought in by photons is very low. Since the experimental data are not available within the energy range $\langle E_\gamma \rangle$ < 11 MeV, the *IR*s are further calculated with the TALYS software

considering different NLD models. It is found that the *IR* clearly depends on the $\langle E_\gamma \rangle$. The increasing and decreasing trends of the IR values appear within the energy range of 8.5 < $\langle E_\gamma \rangle$ <11.0 MeV. Such trends are not only due to the excitation energy effect but also due to the GDR effect. In our experiment, the *IR* value of ^{164m,g}Ho is 0.30 ± 0.08 at $\langle E_\gamma \rangle$ = 12.65 MeV, which is in agreement with both TALYS calculations and the data of Kolev et al. (1995) within the statistical uncertainty. However, the experimental *IR*s provided by Thiep et al. (2011) and Do et al. (2013) are higher than the TALYS calculations at $\langle E_\gamma \rangle$ > 12 MeV.

5 Conclusion

We carried out the experiment to produce ^{164m,g}Ho via photoneutron reaction induced by a laser-accelerated electron beam, in which the IR value of ^{164m,g}Ho is determined by using the activation and offline γ-ray spectrometry technique. However, since the characteristic γ-rays from the isomeric decay of ^{164m}Ho were not successfully observed, we propose to extract the production yields of ^{164m,g}Ho by partitioning counts of photopeak characterizing the ground-state decay. This is different from the approach by extracting the counts of two photopeaks characterizing directly the isomeric and ground states. The production yields of ^{164m,g}Ho were successfully extracted to be (0.45 ± 0.10) × 10^6 and (1.48 ± 0.14) × 10^6 per laser shot. Accordingly, the IR value is calculated to be 0.30 ± 0.08 at $\langle E_\gamma \rangle$ = 12.65 MeV. The IR as a function of $\langle E_\gamma \rangle$ is further calculated with the TALYS software considering different NLD models. It is found that our result is in agreement with both TALYS calculations and the available experimental data within the statistical uncertainty. In addition, the increasing and decreasing trends of the IR values are observed within the energy range of 8.5 < $\langle E_\gamma \rangle$ <11.0 MeV, suggesting that excitation energy is crucial to determine the IR value of ^{164m,g}Ho.

Data availability statement

The original contributions presented in the study are included in the article/Supplementary material; further inquiries can be directed to the corresponding authors.

Author contributions

JZ: Data curation, Formal Analysis, Investigation, Software, Visualization, Writing–original draft. WQ: Data curation, Investigation, Resources, Writing–review and editing. WF: Data curation, Visualization, Writing–review and editing. ZC: Data curation, Software, Writing–review and editing. KL: Data curation, Visualization, Writing–review and editing. CT: Software, Writing–review and editing. XZ: Resources, Writing–review and editing. ZD: Resources, Writing–review and editing. ZZ: Resources, Writing–review and editing. XL: Writing–review and editing. YY: Writing–review and editing. WL: Funding acquisition, Supervision, Writing–review and editing. WZ: Funding acquisition, Supervision, Writing–review and editing.

Funding

The authors declare financial support was received for the research, authorship, and/or publication of this article. This work was supported by the National Key R&D Program of China (Grant No. 2022YFA1603300), the National Natural Science Foundation of China (Grant No. U2230133), the Independent Research Project of the Key Laboratory of Plasma Physics, CAEP (Grant No. JCKYS2021212009), the Open Fund of the Key Laboratory of Nuclear Data, CIAE (Grant No. JCKY2022201C152), the Research Foundation of Education Bureau of Hunan Province, China (No. 22B0453), the Hunan Provincial Natural Science Foundation of China (No. 2023JJ40525), and the Hengyang Municipal Science and Technology Project (No. 202150054076).

Acknowledgments

The authors thank the XingGuang-III operation team for operating the laser system and providing the laser-accelerated electron beam.

Conflict of interest

The authors declare that the research was conducted in the absence of any commercial or financial relationships that could be construed as a potential conflict of interest.

Publisher's note

References

Agostinelli, S., Allison, J., Amako, K., Apostolakis, J., Araujoa, H., Arce, P., et al. (2003). GEANT4-a simulation toolkit. *Nucl. Instrum. Methods Phys. Res. Sect. A* 506 (3), 250–303. doi:10.1016/S0168-9002(03)01368-8

An, G., Chi, Y., Dang, Y., Fu, G., Guo, B., Huang, Y., et al. (2018). High energy and high brightness laser Compton backscattering gamma-ray source at IHEP. *Matter Radiat. Extrem* 3 (4), 219–226. doi:10.1016/j.mre.2018.01.005

Bergère, R., Beil, H., and Veyssière, A. (1968). Photoneutron cross sections of La, Tb, Ho and Ta. *Nucl. Phys.* 121 (2), 463–480. doi:10.1016/0375-9474(68)90433-8

Berman, B. L., Kelly, M. A., Bramblett, R. L., Caldwell, J. T., and Fultz, S. C. (1969). Giant resonance in deformed nuclei: photoneutron cross sections for Eu^{153}, Dd^{160}, Ho^{165}, and W^{186}. *Phys. Rev.* 185 (4), 1576–1590. doi:10.1103/PhysRev.185.1576

Bonnet, T., Comet, M., Denis-Petit, D., Gobet, F., Hannachi, M., Tarisien, M., et al. (2013). Response functions of fuji imaging plates to monoenergetic protons in the energy range 0.6–3.2 MeV. *Rev. Sci. Instrum.* 84 (1), 013508. doi:10.1063/1.4775719

Cao, Z., Qi, W., Lan, H., Cui, B., Zhang, X., Deng, Z., et al. (2023). Experimental study of medical isotopes ^{62,64}Cu and ^{68}Ga production using intense picosecond laser pulse. *Plasma Phys. control. Fusion* 65, 055007. doi:10.1088/1361-6587/acc090

Danson, C., Haefner, C., Bromage, J., Butcher, T., Chanteloup, J., Chowdhury, E., et al. (2019). Petawatt and exawatt class lasers worldwide. *High. Power Laser Sci.* 7, E54. doi:10.1017/hpl.2019.36

Do, N. V., Khue, P. D., Thanh, K. T., Hien, N. T., Kim, G., Lee, M., et al. (2013). Measurement of isomeric yield ratios for the ^{nat}Ho(γ, xn)$^{164m, g; 162m, g}$Ho reactions in the bremsstrahlung energy region from 45 to 65 MeV. *J. Radioanal. Nucl.* 298, 1447–1452. doi:10.1007/s10967-013-2608-6

Fan, W., Qi, W., Zhang, J., Cao, Z., Lan, H., Li, X., et al. (2023). Efficient production of nuclear isomer ^{93m}Mo with laser-accelerated proton beam and an astrophysical implication on ^{92}Mo production. Available at: https://arxiv.org/ftp/arxiv/papers/2308/2308.02994.pdf.

Feng, J., Li, Y., Tan, J., Wang, W., Li, Y., Zhang, X., et al. (2022). *Laser plasma accelerated ultra-intense electron beam for efficiently exciting nuclear isomers*. doi:10.48550/arXiv.2203.06454

Günther, M. M., Rosmej, O. N., Tavana, P., Gyrdymov, M., Skobliakov, A., Kantsyrev, A., et al. (2022). Forward-looking insights in laser-generated ultra-intense γ-ray and neutron sources for nuclear application and science. *Nat. Commun.* 13, 170. doi:10.1038/s41467-021-27694-7

Habs, D., and Köster, U. (2011). Production of medical radioisotopes with high specific activity in photonuclear reactions with γ-beams of high intensity and large brilliance. *Appl. Phys. B* 103, 501–519. doi:10.1007/s00340-010-4278-1

Hayakawa, T., Miyamoto, S., Hayashi, Y., Kawase, K., Horikawa, K., Chiba, S., et al. (2008). Half-life of the 164Ho by the (γ,n) reaction from laser Compton scattering γ rays at the electron storage ring NewSUBARU. *Phys. Rev. C* 74, 065802. doi:10.1103/physrevc.74.065802

Hilgers, K., Qaim, S. M., and Sudar, S. (2007). Formation of the isomeric pairs $^{1^3}$Nd^{m,g} and ^{11}Nd^{m,g} in proton and ^{3}He-particle-induced nuclear reactions. *Phys. Rev. C* 76, 064601. doi:10.1103/PHYSREVC.76.064601

Inagaki, M., Sekimoto, S., Tadokoro, T., Ueno, Y., Kani, Y., Ohtsuki, T., et al. (2020). Production of ^{99}Mo/^{99m}Tc by photonuclear reaction using a $^{nat}MoO_3$ target. *J. Radioanal. Nucl. Chem.* 324, 681–686. doi:10.1007/s10967-020-07086-9

Jacobs, E., Thierens, H., Frenne, D. D., Clercq, A. D., D'hondt, P., Gelder, P. D., et al. (1979). Product yields for the photofission of ^{238}U with 12-15-20-30-and 70-MeV bremsstrahlung. *Phys. Rev. C* 19 (2), 422–432. doi:10.1103/PhysRevC.19.422

Jonsson, G., and Eriksson, M. (1977). Isomeric ratios in photon-induced spallation reactions at intermediate energies. *Z. Phys. A* 281, 53–56. doi:10.1007/BF01408612

Kim, K., Kim, G., Naik, H., Zaman, M., Yang, S., Song, T., et al. (2015). Excitation function and isomeric ratio of Tc-isotopes from the ^{93}Nb(α, xn) reaction. *Nucl. Phys.* 935, 65–78. doi:10.1016/j.nuclphysa.2014.12.006

Kolev, D., Dobreva, E., Nenov, N., and Todorov, V. (1995). A convenient method for experimental determination of yields and isomeric ratios in photonuclear reactions measured by the activation technique. *Nucl. Instrum. Methods Phys. Res. Sect. A* 356 (2-3), 390–396. doi:10.1016/0168-9002(94)01319-5

Koning, A. J., Rochman, D., Sublet, J., Dzysiuk, N., Fleming, M., and Marck, S. V. D. (2019). TENDL: complete nuclear data library for innovative nuclear science and technology. *Nucl. Data Sheets* 155, 1–55. doi:10.1016/j.nds.2019.01.002

Luo, J., and Jiang, L. (2014). Ground-state and isomeric-state cross sections for ^{165}Ho(n, 2n)^{164}Ho reaction from the reaction threshold to 20 MeV. *Phys. Rev. C* 89, 014604. doi:10.1103/PhysRevC.89.014604

Naik, H., Kim, G. N., Schwengner, R., Kim, K., Zaman, M., Yang, S. C., et al. (2016). Measurement of isomeric ratios for ^{89g,m}Zr, ^{91g,m}Mo, and ^{97g,m}Nb in the bremsstrahlung end-point energies of 16 and 45-70 MeV. *Eur. Phys. J.* 52, 47. doi:10.1140/epja/i2016-16047-8

Nishiuchi, M., Sakaki, H., Dover, N. P., Miyahara, T., Shiokawa, K., Manabe, S., et al. (2020). Ion species discrimination method by linear energy transfer measurement in Fujifilm BAS-SR imaging plate. *Rev. Sci. Instrum.* 91, 093305. doi:10.1063/5.0016515

Peik, E., Schumm, T., Safronova, M. S., Pálffy, A., Weitenberg, J., and Thirolf, P. G. (2021). Nuclear clocks for testing fundamental physics. *Quantum Sci. Technol.* 6, 034002. doi:10.1088/2058-9565/abe9c2

Prelas, M. A., Weaver, C. L., Watermann, M. L., Lukosi, E. D., Schott, R. J., and Wisniewskiet, A. (2014). A review of nuclear batteries. *Prog. Nucl. Energ* 75, 117–148. doi:10.1016/j.pnucene.2014.04.007

Qi, W., Zhang, X., Zhang, B., He, S., Zhang, F., Cui, B., et al. (2019). Enhanced photoneutron production by intense picoseconds laser interacting with gas-solid hybrid targets. *Phys. Plasmas.* 26, 043103. doi:10.1063/1.5079773

Rahman, M. S., Kim, K., Kim, G., Naik, H., Nadeem, M., Hien, N. T., et al. (2016). Measurement of flux-weighted average cross-sections and isomeric yield ratios for ^{103}Rh(γ, xn) reactions in the bremsstrahlung end-point energies of 55 and 60 MeV. *Eur. Phys. J. A* 52, 194. doi:10.1140/epja/i2016-16194-x

Rahman, M. S., Kim, K., Nguyen, T. H., Kim, G., Naik, H., Yang, S., et al. (2020). Measurement of flux-weighted average cross sections of ^{nat}In(γ, xn) reactions and isomeric yield ratios of $^{112mg, 111m,g, 110m,g}$ in with bremsstrahlung. *Eur. Phys. J. A* 56, 235. doi:10.1140/epja/s10050-020-00245-2

Robbie, W., Martin, K., Ross, G., David, C., Rachel, D., Nicholas, B., et al. (2018). Development of focusing plasma mirrors for ultraintense laser-driven particle and radiation sources. *Quantum Beam Sci.* 2 (1), 1. doi:10.3390/qubs2010001

Schlenvoigt, H. P., Haupt, K., Debus, A., Budde, F., Jäckel, O., Pfotenhauer, S., et al. (2008). A compact synchrotron radiation source driven by a laser-plasma wakefield accelerator. *Nat. Phys.* 4, 130–133. doi:10.1038/nphys811

Pan, W., Song, T., Lan, H., Ma, Z., Zhang, J., Zhu, Z., and Luo, W. (2021). Photo-excitation production of medically interesting isomers using intense γ-ray source. *Appl Radiat Isotopes* 168, 109534. doi:10.1016/j.apradiso.2020.109534

Singh, B., and Chen, J. (2018). Nuclear data sheets for A=164. *Nucl. Data Sheets* 147, 1–381. doi:10.1016/j.nds.2018.01.001

Thiep, T. D., An, T. T., Cuong, P. V., Vinh, N. T., and Belov, A. G. (2011). Study of the isomeric ratios in photonuclear reactions of natural holmium and lutetium induced by bremsstrahlungs with endpoint energies in the giant dipole resonance region. *J. Radioanal. Nucl. Chem.* 290, 515–524. doi:10.1007/s10967-011-1257-x

Wang, H., Fan, G., Liu, L., Xu, H., Shen, W., Ma, Y., et al. (2022). Commissioning of laser electron gamma beamline SLEGS at SSRF. *Nucl. Sci. Tech.* 33, 87. doi:10.1007/s41365-022-01076-0

Zilges, A., Balabanski, D., Isaak, J., and Pietralla, N. (2022). Photonuclear reactions-From basic research to applications. *Prog. Part. Nucl. Phys.* 122, 103903. doi:10.1016/j.ppnp.2021.103903

10.3389/fspas.2023.1265919

Appendix

The photopeak counts C_x $(x = m,g)$ is the integration of the Activity A_x for x-state considering I_x and ε_x over a detection time t_d as follows:

$$C_x = \int_0^{t_d} I_x \varepsilon_x A_x dt. \tag{A1}$$

As shown above, the activity A_x is the key factor in the C_x solution. According to Eq. 1 in the proof (on line 204), in irradiation interval, both the productions and the decay properties contribute to the activities of the isomeric and ground states. And in the cooling and the detection interval, only the decay properties of two states contribute to the activities. So, we deduce the activities of the isomeric and ground states for two intervals, i.e., the irradiation interval and the natural decay interval (including cooling interval and detection interval).

Firstly, the number of x-state N_x at the irradiation time t_{irr} can be solved out. In irradiation interval, the N_x changes as a function of t_{irr} and the formula is like to Eq. 1 in the proof. By solving the Eq. 1 in the proof, the N_x at the irradiation time t_{irr} can be obtained as:

$$N_m = \frac{1}{\lambda_m} p_m \left(1 - e^{-\lambda_m t_{irr}}\right), \tag{A2}$$

$$N_g = \eta p_m \frac{1}{\lambda_g\left(\lambda_g - \lambda_m\right)}\left(\lambda_g\left(1 - e^{-\lambda_m t_{irr}}\right) - \lambda_m\left(1 - e^{-\lambda_g t_{irr}}\right)\right) + \frac{1}{\lambda_g} p_g\left(1 - e^{-\lambda_g t_{irr}}\right). \tag{A3}$$

And then, in the cooling and the detection intervals, the production doesn't do any contribution to the activities of the isomeric and ground states. Therefore, the Eq. 1 in the proof for the cooling and detection intervals can be written as:

$$\begin{cases} \dfrac{dN_m}{dt} = -\lambda_m N_m, \\ \dfrac{dN_g}{dt} = \eta\lambda_m N_m - \lambda_g N_g. \end{cases} \tag{A4}$$

By solving it, the N_x changes as a function of the cooling t_c and the detection t_d times can be obtained as:

$$N_m = \frac{1}{\lambda_m} p_m \left(1 - e^{-\lambda_m t_{irr}}\right) e^{-\lambda_m t_d} e^{-\lambda_m t_m}, \tag{A5}$$

$$N_g = \frac{\eta_m p_m}{\lambda_g\left(\lambda_g - \lambda_m\right)}\left(\lambda_g\left(1 - e^{-\lambda_m t_{irr}}\right) e^{-\lambda_m t_c} e^{-\lambda_m t_d} - \lambda_m\left(1 - e^{-\lambda_g t_{irr}}\right) \times e^{-\lambda_g t_c} e^{-\lambda_g t_d}\right) + \frac{1}{\lambda_g} p_g\left(1 - e^{-\lambda_g t_{irr}}\right) e^{-\lambda_g t_c} e^{-\lambda_g t_d}. \tag{A6}$$

Due to $A_x = \lambda_x N_x$, the A_x can be obtained as the following:

$$A_m = p_m \left(1 - e^{-\lambda_m t_{irr}}\right) e^{-\lambda_m t_d} e^{-\lambda_m t_m}, \tag{A7}$$

$$A_g = \frac{\eta_m p_m}{\left(\lambda_g - \lambda_m\right)}\left(\lambda_g\left(1 - e^{-\lambda_m t_{irr}}\right) e^{-\lambda_m t_c} e^{-\lambda_m t_d} - \lambda_m\left(1 - e^{-\lambda_g t_{irr}}\right) \times e^{-\lambda_g t_c} e^{-\lambda_g t_d}\right) + p_g\left(1 - e^{-\lambda_g t_{irr}}\right) e^{-\lambda_g t_c} e^{-\lambda_g t_d}. \tag{A8}$$

Substituting Eq. 7 into Eq. 1 and solving it, the C_m can be gotten as:

$$C_m = I_m \varepsilon_m p_m \frac{\left(1 - e^{-\lambda_m t_{irr}}\right)}{\lambda_m} e^{-\lambda_m t_c}\left(1 - e^{-\lambda_m t_d}\right), \tag{A9}$$

where the Eq. 3a in the proof is deduced out.

And do the same performance to Eq. 8 like Eq. 7. The C_g can be obtained as:

$$C_g = I_g \varepsilon_g \left\{ p_g \frac{1 - e^{-\lambda_g t_{irr}}}{\lambda_g} e^{-\lambda_g t_c}\left(1 - e^{-\lambda_g t_d}\right) + p_m \frac{\eta}{\lambda_g - \lambda_m}\left[\frac{\lambda_g}{\lambda_m}\left(1 - e^{-\lambda_m t_{irr}}\right) \times e^{-\lambda_m t_c}\left(1 - e^{-\lambda_m t_d}\right) - \frac{\lambda_m}{\lambda_g}\left(1 - e^{-\lambda_g t_{irr}}\right) e^{-\lambda_g t_c}\left(1 - e^{-\lambda_g t_d}\right)\right]\right\}, \tag{A10}$$

where the Eq. 3b in the proof is deduced out.